Mitochondrial immobilization mediated by syntaphilin facilitates survival of demyelinated axons

Nobuhiko Ohno[a,1], Hao Chiang[a,2], Don J. Mahad[a,3], Grahame J. Kidd[a], LiPing Liu[a], Richard M. Ransohoff[a], Zu-Hang Sheng[b], Hitoshi Komuro[a], and Bruce D. Trapp[a,4]

[a]Department of Neurosciences, Lerner Research Institute, Cleveland Clinic, Cleveland, OH 44195; and [b]Synaptic Function Section, National Institute of Neurological Disorders and Stroke, National Institutes of Health, Bethesda, MD 20892

Axonal degeneration is a primary cause of permanent neurological disability in individuals with the CNS demyelinating disease multiple sclerosis. Dysfunction of axonal mitochondria and imbalanced energy demand and supply are implicated in degeneration of chronically demyelinated axons. The purpose of this study was to define the roles of mitochondrial volume and distribution in axonal degeneration following acute CNS demyelination. We show that the axonal mitochondrial volume increase following acute demyelination of WT CNS axons does not occur in demyelinated axons deficient in syntaphilin, an axonal molecule that immobilizes stationary mitochondria to microtubules. These findings were supported by time-lapse imaging of WT and syntaphilin-deficient axons in vitro. When demyelinated, axons deficient in syntaphilin degenerate at a significantly greater rate than WT axons, and this degeneration can be rescued by reducing axonal electrical activity with the Na$^+$ channel blocker flecainide. These results support the concept that syntaphilin-mediated immobilization of mitochondria to microtubules is required for the volume increase of axonal mitochondria following acute demyelination and protects against axonal degeneration in the CNS.

Axonal loss is the major cause of permanent neurological disability in individuals with primary diseases of myelin (1). Axonal degeneration associated with myelin diseases has been well studied in the immune-mediated CNS demyelinating disease multiple sclerosis. Two mechanisms are responsible for the degeneration of demyelinated axons in multiple sclerosis brains. First, axons are transected in acute multiple sclerosis lesions (2) and axonal injury correlates with the number of infiltrating peripheral immune cells (3, 4). Edema associated with breakdown of the blood–brain barrier and toxic substances secreted by inflammatory immune cells are thought to transect the acutely demyelinated axon (5). Second, chronically demyelinated axons degenerate as a result of loss of trophic support provided by oligodendrocytes and myelin (6, 7). In addition to increasing the speed of nerve transmission, oligodendrocytes and myelin provide axons with trophic support that is essential for their long-term survival (8–10). Although most demyelinated axons compensate for loss of oligodendrocytes/myelin, additional insults to axonal mitochondria impair axonal metabolism, increase axonal Ca^{2+}, and promote progressive disruption of mitochondrial function (11, 12). Changes in axonal mitochondria have been described in chronically demyelinated axons in postmortem multiple sclerosis tissue, and include decreased expression of nuclear-encoded mitochondrial genes (13), reduced mitochondrial respiration (14), and genetic alterations in mitochondrial DNA (15). A vicious cycle of reduced ATP production and increased axonal Ca^{2+} results in degeneration of the chronically demyelinated axon.

Myelinated axons contain two populations of mitochondria. Most axonal mitochondria do not appear to translocate and are located at stationary sites. Mitochondrial stationary sites are distributed along the entire length of the axon, and individual sites can have multiple mitochondria that may vary in length but not in diameter (16–19). In live imaging studies, a population of relatively small axonal mitochondria is translocated in

anterograde and retrograde directions (17, 18, 20). Motile mitochondria are made in the neuronal cell body, can transiently stop within stationary sites, and can fuse with or bud from stationary mitochondria; they are essential for axonal mitochondria turnover and redistribution (20–23). Transport and docking of axonal mitochondria are dynamic processes that can be modulated by axonal metabolic demands. For example, mitochondrial stationary sites can be increased in nodal axoplasm by increased axonal firing (18).

Syntaphilin tethers and immobilizes axonal mitochondria to microtubules at stationary sites (24). In syntaphilin-null unmyelinated axons in vitro, mitochondrial stationary site volume is decreased and the number of motile mitochondria is increased (24). Overexpression of syntaphilin increased axonal stationary site size and reduced the number of motile mitochondria (25). The purpose of the present study is twofold. First, we investigated whether axonal degeneration was a feature of acute toxin-induced CNS demyelination. Second, we investigated the role of axonal mitochondria in the axonal pathology associated with acute toxin-mediated CNS demyelination by comparing mitochondrial distribution/shape and axonal pathology in WT and syntaphilin-deficient demyelinated axons.

Significance

Degeneration of demyelinated axons is a major cause of permanent neurological disability in primary diseases of myelin. In addition to myelin loss, dysfunction of axonal mitochondria may be an essential requisite for degeneration of demyelinated axons. Here we describe a significant increase in axonal mitochondrial volume following demyelination of CNS axons. A deficiency in tethering mitochondria to the cytoskeleton prevented this volume increase in demyelinated axons and increased axonal degeneration, which was rescued by pharmacological inhibition of nerve transmission along the demyelinated axon. These results demonstrate that (i) increasing mitochondrial volume in CNS demyelinated axons protects against axonal degeneration and (ii) immobilization of mitochondria is required for the increase in axonal mitochondria volume following CNS demyelination.

NEUROSCIENCE

www.manaraa.com

As demonstrated previously in demyelinated peripheral nervous system (PNS) axons (17), we find that the volume of mitochondrial stationary sites is increased in demyelinated CNS axons. We extend this observation by demonstrating that syntaphilin plays an essential role in increasing mitochondrial stationary site size in CNS demyelinated axons. Failure to increase mitochondrial stationary sites following demyelination of syntaphilin-deficient axons increased axonal degeneration and axonal pathology. Degeneration of syntaphilin-null demyelinated axons was reduced by treatment with the Na$^+$ channel blocker flecainide. These results support the concept that syntaphilin-mediated mitochondrial immobilization is essential for increasing the size of mitochondrial stationary sites in demyelinated axons. Increased mitochondrial volume is an adaptive response of the demyelinated axon, which helps meet the increased energy demands of nonsaltatory nerve conduction and minimizes axonal degeneration and the progression of neurological disability.

Results

The purpose of this study is to compare mitochondrial distribution/shape and axonal pathology in WT and syntaphilin-deficient demyelinated axons. We first investigated whether the number of myelinated fibers and the distribution/size of mitochondria in myelinated axons were similar in WT and syntaphilin-null corpus callosa. We chose the corpus callosum because it is a common target of demyelination in multiple sclerosis brains (26) and is extensively demyelinated in cuprizone-fed mice. By using serial block face scanning EM, we quantified myelinated axons and compared the 3D size and distribution of individual mitochondria in myelinated and demyelinated corpus callosa from WT and syntaphilin-null mice (Fig. 1 A–G). The size and density of myelinated fibers (Fig. 1 A and C) was similar in WT and syntaphilin-deficient corpus callosa. Mitochondrial number per myelinated axonal volume (Fig. 1K) and mitochondrial volume per myelinated axonal volume (Fig. 1L) were similar in WT and syntaphilin-null corpus callosa; we used total axonal volume instead of axonal length as the denominator to allow for any differences in axon diameter among sample sets. Volumes (Fig. 1H) and lengths (Fig. 1I) of individual axonal mitochondria were also similar. Compared with WT myelinated axons, there was a slight but significant decrease in the diameter of mitochondria (Fig. 1J) in syntaphilin-null myelinated axons. Similar densities and volumes of axonal mitochondria and the absence of major neurological phenotypes (24) indicate that the mouse neuron/axon can compensate for loss of syntaphilin during the first four postnatal months.

We next investigated how WT and syntaphilin-null axons responded to demyelination induced by cuprizone/rapamycin treatment. Cuprizone is a toxin that kills oligodendrocytes (27). During a 6-wk cuprizone feeding paradigm, spontaneous remyelination of the corpus callosum occurs by 4 wk of cuprizone-only treatment. Cuprizone, however, does not kill these remyelinating oligodendrocytes. This remyelination can, however, be inhibited by daily concurrent injections of rapamycin (28). The combination of cuprizone feeding and daily rapamycin injections for 6 wk demyelinates the corpus callosum (Fig. 1B). All control mice received daily rapamycin injections in these experiments. Demyelination was extensive in WT and syntaphilin-null corpus callosa (Fig. 1C). In WT demyelinated axons, the volumes (Fig. 1H) and lengths (Fig. 1I) of individual mitochondria and mitochondrial number per axonal volume (Fig. 1K) were significantly increased, and mitochondrial volume per axonal volume (Fig. 1L) was doubled compared with myelinated WT axons. In contrast, neither the volume of individual mitochondria (Fig. 1H) nor mitochondrial numbers per axonal volume (Fig. 1K) were increased in demyelinated syntaphilin-null axons in which mitochondria were ~50% shorter (Fig. 1I) and ~50% wider (Fig. 1J) compared with myelinated syntaphilin-null axons. Thus, unlike WT demyelinated axons, syntaphilin-null axons
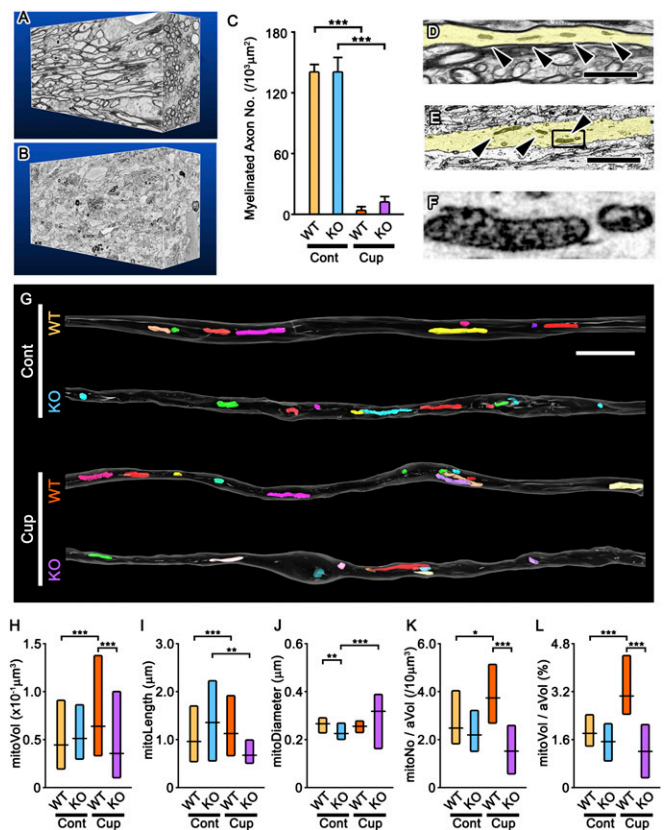

Fig. 1. Syntaphilin is essential for increasing mitochondrial stationary site size in demyelinated CNS axons. (A and B) Three-dimensional reconstructions of serial EM images of myelinated (A) and demyelinated (B) corpus callosa from syntaphilin-null mice. (C) The number of myelinated axons is similar in WT and syntaphilin-null (KO) corpus callosa. Demyelination following cuprizone treatment (Cup) is almost complete in both strains of mice (n = 8 for Control and n = 10 for Cup; ***P < 0.001, t test). (D–F) Individual slices illustrating mitochondria (arrowheads) in myelinated (D) and demyelinated (E and F) axons (yellow) from syntaphilin-KO mice. (G) Three-dimensional reconstructions of individual axonal mitochondria (various colors) in corpus callosum of myelinated (Cont) and demyelinated (Cup) WT and syntaphilin-null (KO) mice. (H–J) Compared with mitochondria in WT myelinated axons, mitochondria in WT demyelinated axons were significantly larger (H) and longer (I). In contrast, mitochondria in syntaphilin-null demyelinated axons were similar in volume (H), but shorter (I) and thicker (J) than mitochondria in myelinated syntaphilin-null axons. (K and L) Percent axonal volume occupied by mitochondria (mitoVol/aVol; L) and mitochondrial density (mitoNo/aVol; K) are similar in myelinated WT axons compared with myelinated syntaphilin-null axons. Percent axonal volume occupied by mitochondria and mitochondrial density are increased in demyelinated WT axons but are unchanged in demyelinated syntaphilin-null axons. Medians (lines) and first-to-third quartile ranges (boxes) are shown (*P < 0.05, **P < 0.01, and ***P < 0.001). For control/WT, control/KO, cuprizone/WT, and cuprizone/KO, n = 207, n = 134, n = 320, and n = 128 mitochondria (H–J), respectively, and n = 24, n = 18, n = 26, and n = 24 axons (K and L), respectively. (Scale bars: 3 μm.)

did not increase mitochondrial volume per axonal volume following demyelination (Fig. 1L). High doses of cuprizone delivered to weanling mice have profound effects in hepatocytes, producing swollen "giant" mitochondria characterized by fragmented short cristae concentrated at the periphery of the swollen mitochondria (29, 30). Following 6 wk of cuprizone/rapamycin treatment, giant mitochondria with fragmented cristae were not found in WT (Fig. S1A) or syntaphilin-null axons (Fig. S1B), including regions with axonal swellings. Swollen axonal mitochondria with altered cristae were not detected in previous studies using similar cuprizone dosing
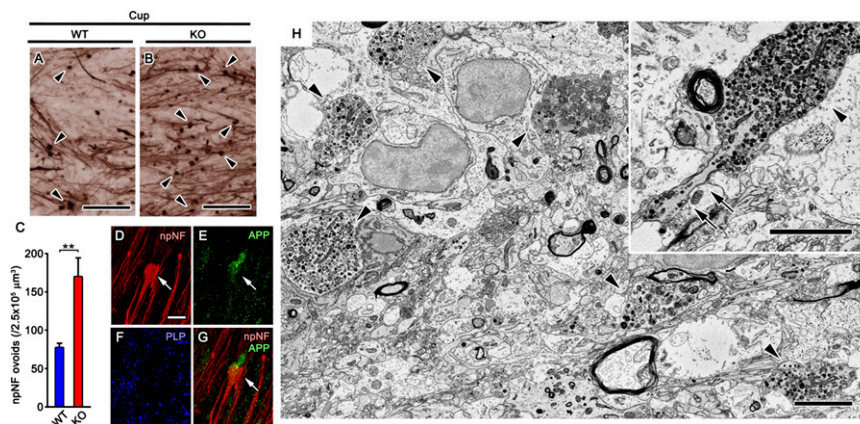
Fig. 2. Axonal ovoids are increased in demyelinated syntaphilin-null CNS axons. (*A* and *B*) Immunostaining for nonphosphorylated neurofilament (npNF) in demyelinated corpus callosum of WT (*A*) and syntaphilin-null (KO) mice (*B*). (*C*) The number of axonal ovoids (*A* and *B*, arrowheads) is significantly increased in demyelinated corpus callosum of syntaphilin-null mice (**P < 0.01; *n* = 7 WT mice; *n* = 5 KO mice). (*D–G*) Immunostaining for nonphosphorylated neurofilament (red), APP (green), and proteolipid protein (PLP, blue) shows that APP accumulates in axonal ovoids (arrows) in demyelinated syntaphilin-null corpus callosum. (*H*) EM images obtained from demyelinated corpus callosum from syntaphilin-null mice show multiple axonal ovoids filled with membranous organelles (arrowheads). (*I*) Ovoid attached to a thin axon (arrows). (Scale bars: *A* and *B*, 100 μm; *D*, 10 μm; *H*, 5 μm.)

paradigms (31, 32). Mitochondria in hepatocytes in our cuprizone/rapamycin-treated mice, however, were slightly swollen with altered cristae distributions (Fig. S1 *C and D*). This differential effect on hepatocyte mitochondria reflects the detoxifying role of liver. These observations demonstrate that the cuprizone treatment in the present study does not alter mitochondrial structure in CNS axons and indicate that syntaphilin is required for the increase in mitochondrial size and density that occurs after demyelination of CNS axons.

We next asked whether the lack of syntaphilin promotes axonal degeneration in the demyelinated corpus callosa. Degeneration of demyelinated axons was assessed by comparing the number of nonphosphorylated neurofilament-positive axonal ovoids in demyelinated corpus callosa from WT (Fig. 2*A*) and syntaphilin-null (Fig. 2*B*) mice. These ovoids represent the cut ends of axons that are still connected to viable neurons (2) or axonal swellings that precede axonal transection (33, 34). Axonal ovoids positive for nonphosphorylated neurofilament were not observed in myelinated corpus callosa of WT and syntaphilin-deficient mice. Axonal ovoids were significantly increased and twice as common in syntaphilin-null demyelinated corpus callosa compared with WT (Fig. 2*C*), and 70.0 ± 5.5% (*n* = 5 corpus callosa) of axonal ovoids contained detectable levels of the amyloid precursor protein (APP; Fig. 2 *D–G*), a marker for compromised axonal transport (3, 4, 35). Axonal ovoids were readily identified in EM images of corpus callosum (Fig. 2*H*) and contained densely packed axoplasmic organelles, including intact and fragmented mitochondria. Axonal ovoids were more frequent and approximately three times larger in EM images of demyelinated syntaphilin-KO mice compared with demyelinated WT mice. In EM analyses, axonal ovoids were not found in myelinated WT and syntaphilin-KO mice (Fig. S2). These results show that axonal ovoid formation is increased in demyelinated syntaphilin-deficient axons.

We next compared axonal DsRed2-labeled mitochondrial distribution and transport in myelinated and demyelinated living cerebellar slice cultures from WT and syntaphilin-deficient mice (Fig. 3*A*). In these slice cultures, the majority of axonal mitochondria were stationary, and the size of mitochondrial stationary sites was similar in WT and syntaphilin-deficient myelinated axons (Fig. 3*B*). The number of motile mitochondria, however, was increased in syntaphilin-deficient myelinated axons compared with myelinated WT axons (Fig. 3*C* and Fig. S3), but their mean velocity of mitochondrial transport was similar (Fig. 3*C*

and Fig. S3). Mitochondrial stationary site size (Fig. 3*B*), the number of motile mitochondria (Fig. 3*C*), and the velocity of mitochondrial transport (Fig. 3*D*) were significantly increased in demyelinated WT axons compared with WT myelinated axons. In contrast, mitochondria stationary site size was similar in myelinated and demyelinated syntaphilin-deficient axons (Fig. 3*B*). The number of motile mitochondria (Fig. 3*C*) and the mean velocity of motile mitochondria translocation (Fig. 3*D*) were significantly decreased in demyelinated syntaphilin-deficient axons compared with myelinated syntaphilin-deficient axons.

To examine axonal pathology in the slice cultures, myelinated and demyelinated WT and syntaphilin-deficient cerebellar cultures were immunostained for neurofilaments and APP (3, 4, 35). Although the number of APP-positive axonal ovoids in myelinated WT slices was comparable to that in myelinated syntaphilin-deficient slices, demyelinated syntaphilin-deficient slices had significantly more APP-positive axonal ovoids and transections than demyelinated WT slices and myelinated syntaphilin-deficient slices (Fig. 4). Increased axonal pathology in demyelinated syntaphilin-deficient axons was also found in demyelinated corpus callosa of syntaphilin-KO mice (Fig. 2 and Fig. S2). Na$^+$ channel blockers can reduce axonal pathology in conditions that compromise axonal mitochondrial energy production (36, 37). If reduced mitochondrial density in syntaphilin-deficient axons leads to insufficient energy production for axonal survival, blocking Na$^+$-channel activities may be beneficial for the survival of demyelinated syntaphilin-deficient axons. Flecainide is a Na$^+$ channel blocker that can reduce axonal loss following NO treatment in vitro and during inflammatory demyelination in vivo (37, 38). Indeed, when syntaphilin-deficient slice cultures were treated with flecainide, APP-positive axonal ovoids and transections were significantly decreased in a dose-dependent manner (Fig. 4*G*). These in vitro results collectively demonstrate that syntaphilin plays an important role in increasing the volume of axonal mitochondrial stationary sites upon demyelination, and provides further support to the hypothesis that increased mitochondrial stationary site size protects against degeneration of demyelinated axons, which is caused in part by the increased energy demands of nonsaltatory nerve conduction.

Discussion

The present study investigated mitochondrial behavior in acutely demyelinated CNS axons. We described changes in mitochondrial distribution in demyelinated axons in vivo by using 3D EM
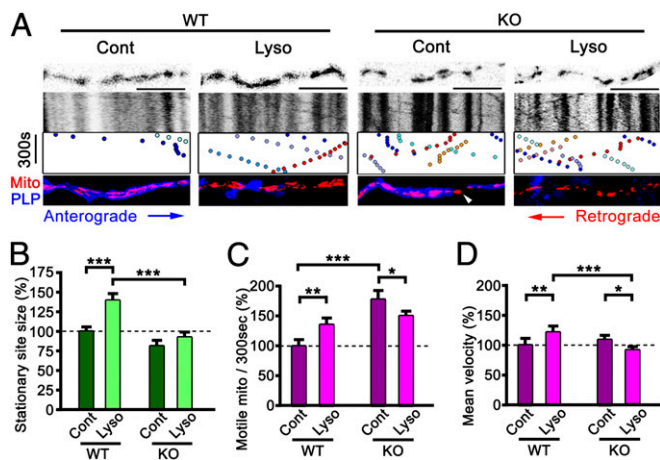
Ohno et al.

NEUROSCIENCE

Fig. 3. Mitochondrial behavior in myelinated and demyelinated WT and syntaphilin-null axons in vitro. (*A, Upper*) Mito-DsRed distribution in projected staked images of living myelinated (Cont) and demyelinated (Lyso) WT and syntaphilin-deficient (KO) slice cultures. (*A, Middle*) Kymographs of staked images show stationary sites as vertical black lines and trajectories of mobile mitochondria as colored dots. (*A, Lower*) Following live imaging, slices were fixed and stained for proteolipid protein (blue) to confirm myelination and demyelination of imaged axons. Mitochondria distribution is shown in red. (*B–D*) In contrast to demyelinated WT axons, demyelinated syntaphilin-null axons do not increase mitochondrial stationary site sizes (*B*), the number of motile mitochondria (*C*), or the speed of mitochondria transport (*D*). Compared with myelinated WT axons, motile mitochondria are increased in myelinated syntaphilin-null axons (*C*). (Scale bars: 10 μm.) Bars in *B–D* represent means and SEM (*$P < 0.05$, **$P < 0.01$, and ***$P < 0.001$). For WT-Cont, WT-Lyso, KO-Cont, and KO-Lyso, $n = 17$, $n = 16$, $n = 19$, and $n = 19$ axons (*B*), respectively, and $n = 14$, $n = 16$, $n = 19$, and $n = 17$ (*C* and *D*) axons.

and visualized mitochondrial motility and distribution in living myelinated and demyelinated CNS axons in vitro. As we previously described for demyelinated PNS axons in vitro (17), CNS demyelinated axons compensate for loss of myelin by increasing (*i*) the volume of mitochondrial stationary sites and (*ii*) the number and velocity of motile mitochondrial transport. By using syntaphilin-deficient mice, we extend these fundamental mitochondrial responses shared by CNS and PNS demyelinated axons by establishing that (*i*) syntaphilin-mediated immobilization of stationary mitochondria is essential for the increased volume of mitochondrial stationary sites in demyelinated CNS axons, (*ii*) deleting axonal syntaphilin significantly increases degeneration of demyelinated CNS axons, and (*iii*) the incidence of this axonal degeneration can be reduced by blocking Na$^+$ channel activity. Collectively, our studies indicate that acutely demyelinated axons increase the volume of mitochondrial stationary sites to meet the increased energy demands of nonsaltatory nerve conduction and thereby prevent or slow axonal degeneration.

Lack of significant behavioral or neurological phenotypes (24) and no change of mitochondrial density and volume in syntaphilin-null mice at 2–3 mo of age indicate that myelinated axons can compensate for the loss of syntaphilin during development and early postnatal life. The mechanism by which this compensation occurs is unknown. In contrast, we establish that syntaphilin-null axons cannot fully compensate for loss of myelin. Specifically, demyelinated syntaphilin-null axons do not increase the size of stationary mitochondria, but they contain more ovoids and they degenerated at a greater rate than demyelinated WT axons. The frequent presence of axonal ovoids positive for APP support that axonal ovoid formation in demyelinated syntaphilin-null axons accompanies impaired axonal transport (3, 4, 35). Mitochondrial biogenesis and/or redistribution in addition to an imbalance between mitochondrial fusion/fission are likely to be

responsible for the increase of stationary mitochondria volume in demyelinated axons. Syntaphilin immunoreactivity is increased in demyelinated lesions in postmortem brains obtained from individuals with multiple sclerosis, and this increased staining is associated with mitochondria (14). A similar increase in syntaphilin-positive mitochondria was found in demyelinated axons in the present study (Fig. S4). Mitochondria in syntaphilin-null demyelinated axons were shorter and thicker than those in demyelinated WT axons. Syntaphilin appears to be required for the rapid increase in stationary mitochondrial volume that occurs through interactions with microtubules following demyelination. Further studies are necessary to address how syntaphilin is regulated in demyelinated axons and how syntaphilin-mediated mitochondrial immobilization indirectly affects mitochondrial fusion/fission to facilitate mitochondrial elongation.

An important question in the present study is whether cuprizone alters mitochondria function in demyelinated axons. To address this question, we used 3D EM to investigate whether mitochondrial pathologic conditions described in liver (29, 30) were present in demyelinated axons in cuprizone/rapamycin-treated mice. Consistent with previous studies that used similar concentrations of cuprizone (0.2–0.3%) to demyelinate CNS axons (31, 32), we did not detect swollen mitochondria with peripherally located cisternae in WT or syntaphilin-null demyelinated axons. The cuprizone doses used to cause giant mitochondria in liver were 60–300% greater than that used in the present study, and the mice were much younger and thus more susceptible to cuprizone toxicity (27, 39). In contrast to the CNS, we did detect abnormal mitochondria in the liver from our cuprizone/rapamycin-treated mice (Fig. S1). Hepatocyte mitochondria from cuprizone/rapamycin-treated mice were swollen and contained abnormally distributed cisternae compared with mitochondria in hepatocytes from mice that received rapamycin only (Fig. S1 *D* and *E*). Their diameter never exceeded 2 μm and never approached diameters reported in the literature (>10 μm diameter) from younger mice receiving higher cuprizone doses. The cuprizone dose used in the present study does not cause changes in mitochondrial structure in CNS axons. Although we cannot rule out cuprizone-induced changes in mitochondrial function, increased mitochondrial size/volume in demyelinated axons has been reported in multiple studies regardless of the cause of demyelination (14, 17, 40–42). The mitochondrial changes described following cuprizone-induced demyelination in vivo were also found following lysolecithin-induced demyelination in vitro. The observation that lysolecithin did not alter mitochondrial behavior in unmyelinated axons provides additional support for demyelination (not cuprizone-induced mitochondria changes) as the cause of the changes in axonal mitochondria described in the present paper.

Studies of postmortem multiple sclerosis brains have described increased mitochondria volume in axons that are likely to be demyelinated for years or decades (14, 42). We establish here that increased axonal mitochondrial volume occurs within days (slice cultures) or weeks (mice) of demyelination, and that this increase is caused by increased sizes of mitochondrial stationary sites. Further studies are necessary to elucidate the mechanisms that simultaneously regulate mitochondrial stationary site size and mitochondrial motility in demyelinated axons. To compensate for loss of myelin, the demyelinated axon distributes voltage-gated Na$^+$ channels along its entire surface (43). In contrast to nerve impulses that jump from node to node in myelinated axons, nerve impulses are propagated by continuous depolarization of the axolemma in demyelinated axons. It has been hypothesized that this increases the energy demand for repolarization of the axolemma, which occurs by exchange of axoplasmic Na$^+$ for extracellular K$^+$ in an energy-dependent manner. In addition to increasing the energy demand of nerve conduction, demyelination may also decrease the availability of ATP precursors. Recent studies have raised the
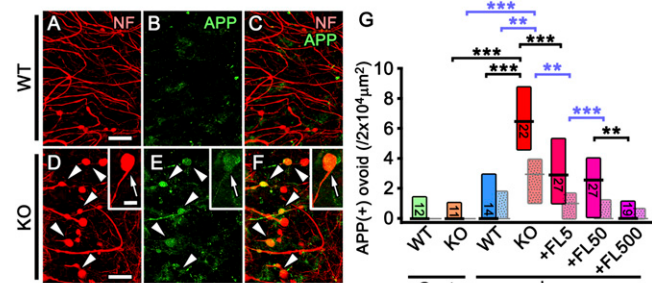
Fig. 4. Na$^+$ channel blockers reduce axonal ovoid formation in syntaphilin-null axons. (*A–F*) Neurofilament (NF, red) and APP (green) immunostaining in organotypic slice cultures prepared from WT and syntaphilin-KO mice and demyelinated with lysolecithin treatment (Lyso). (*Insets*) Transected APP-positive axonal ovoids. (*G*) The number of APP-positive axonal ovoids (black lines and asterisks) and transected APP-positive axonal ovoids (stippled boxes, blue lines, and asterisks) in lysolecithin/KO is significantly increased compared with KO cultures without lysolecithin treatment (Cont) and lysolecithin/WT cultures. The number of APP-positive ovoids in lysolecithin/KO cultures is decreased by flecainide treatment in a dose-dependent manner [5 μM (+FL5), 50 μM (+FL50), and 500 μM (+FL500) flecainide]. Bars show medians (lines) and first-to-third quartile ranges (boxes). (***P* < 0.01 and ****P* < 0.001, *U* test.) Number of samples is shown on each box. (Scale bars: *A* and *D*, 20 μm; *D*, *Inset*, 20 μm.)

possibility that the monocarboxylase transporter-1 located in myelin transfers lactate from the oligodendrocytes to myelinated axons (44, 45). Axons are at risk to degenerate when they cannot generate sufficient ATP to exchange Na$^+$ for K$^+$, as excessive axoplasmic Na$^+$ is exchanged for extracellular Ca^{2+} by the Na$^+$/Ca^{2+} exchanger in an energy-independent manner (12, 46). Increased axoplasmic Ca^{2+} is thought to be a major cause of pathology and degeneration of demyelinated axons (11). We propose, therefore, that failure to increase mitochondrial volume in syntaphilin-deficient demyelinated axons reduces ATP production, increases axonal Na$^+$ and Ca^{2+}, and augments axonal degeneration. This interpretation is consistent with previous studies that have shown that the lack of syntaphilin-mediated mitochondrial docking in presynaptic terminals induces rapid buildup of intracellular Ca^{2+} during intensive stimulation without significantly affecting basal synaptic transmission (24).

ATP output in individual demyelinated axons cannot be reliably measured. We rationalized that the increased energy demand would be proportional to the rate of axonal firing in demyelinated axons. This hypothesis is supported by our observation that blocking Na$^+$ channels of syntaphilin-null demyelinated axons significantly reduced axonal degeneration. This is consistent with previous reports that Na$^+$ channel blockers reduced axonal degeneration in the immune-mediated demyelinating mouse models of experimental autoimmune encephalomyelitis and neuritis (38, 47, 48) and in myelinated peripheral axons treated with NO (37). Given that glutamate-mediated excitotoxicity has been implicated in damage of demyelinated axons (49), stationary mitochondria may also have a direct beneficial role to buffer axoplasmic Ca^{2+} in demyelinated axons, and this buffering capacity may be compromised in syntaphilin-deficient axons. In addition, blockage of axonal Na$^+$ channels can also reduce Ca^{2+} influx and Ca^{2+} signaling pathways that alter axonal stability. Our studies have described mitochondrial changes in demyelinated axons that could involve mitochondrial biogenesis, redistribution, and dynamics, and can render the demyelinated axon more susceptible to axonal degeneration. They raise the possibility that therapeutic stabilization of mitochondria–microtubule docking interactions may prevent or reduce degeneration of demyelinated axons.

Ohno et al.

Materials and Methods

Animals. C57BL/6J mice were purchased from Jackson Laboratories. Syntaphilin-KO mice were generated by Zu-Hang Sheng (24), backcrossed with C57BL/6J mice for more than 12 generations, and genotyped as described previously (24). Animal experimental protocols were approved by the Cleveland Clinic Institutional Animal Care and Use Committee.

In Vivo Demyelination. Demyelination of the corpus callosum was induced by feeding 2–3-mo-old WT and syntaphilin-null mice standard chow containing 0.3% bis(cyclohexanone)oxaldihydrazone (cuprizone; Sigma-Aldrich) for 6 wk. All mice received daily injections of rapamycin (10 mg/kg). Control mice (WT and syntaphilin-deficient) were fed standard rodent chow and received daily injections of rapamycin for 6 wk.

For light microscopic analyses, mice were perfused with 4% (wt/vol) paraformaldehyde, and free-floating sections containing identical areas of the corpus callosum were immunostained as previously described (10). Axonal ovoids (>3 μm in diameter), identified with nonphosphorylated neurofilament (SMI-32; Covance) and β-APP (Invitrogen) antibodies, were quantified and expressed as number per unit area. Free-floating sections of myelinated and demyelinated axons were also stained with syntaphilin antibodies.

Myelinated and demyelinated corpus callosa were analyzed by 3D EM. Mice were perfused with 2.5% (wt/vol) glutaraldehyde and 4% paraformaldehyde, and corpus callosa were removed, stained with heavy metals, and embedded in resin as previously described (18). Serial block-face scanning EM of corpus callosa was performed by using a SigmaVP scanning electron microscope (Carl Zeiss) equipped with a 3View in-chamber ultramicrotome system (Gatan). Serial image sequences were generated at 50–75-nm steps, providing image stacks >10 μm deep and 48 μm × 48 μm wide at a resolution of 5–10 nm per pixel. Images were processed and measured with ImageJ using FIJI plugins (http://fiji.sc/wiki/index.php/Fiji), including TrakEM2 (50). Myelinated axons and demyelinated axons (>0.3 μm in diameter) were quantified. Axonal mitochondria were reconstructed in 3D, and their distribution, length, width, and volume per axonal length/volume were determined. Axonal ovoids were also quantified and measured.

In Vitro Demyelination. Myelinating cerebellar organotypic slice cultures from P8-9 WT and syntaphilin-KO mice were generated, and Purkinje cells were infected with lentiviral constructs containing mitochondria-targeted DsRed2 as reported previously (18). To induce demyelination, slices were incubated with media containing 0.05% wt/vol lysolecithin (L-α-lysophosphatidylcholine; Sigma-Aldrich) for 26 h and maintained without lysolecithin for ~24 h before time-lapse imaging and/or fixation (51). The effect of 0.05% lysolecithin to axons is largely attributable to demyelination, as there is no significant effect on unmyelinated axons (17). Additional WT and syntaphilin-deficient demyelinated slices were treated with 5 μM, 50 μM, or 500 μM flecainide acetate (F6777; Sigma-Aldrich) during the 24 h before fixation.

Time-Lapse Imaging by Confocal Microscopy. The distribution, size, and mean transport velocity of DsRed2-positive mitochondria in myelinated and demyelinated Purkinje cell axons were imaged with a Leica inverted confocal microscope as described previously (18). Total live imaging time was restricted to <20 min to minimize phototoxic damage. Lengths, areas, and diameters of axonal mitochondria were measured by using ImageJ after thresholding. The number and mean velocity of motile mitochondria were extrapolated from kymographs (18). Stationary sites in this study were defined as DsRed-positive profiles that were stationary during a 5-min period. To measure the size of the stationary sites, a pair of image stacks, including all DsRed-positive profiles of each axon, were obtained at time 0 and time 5 min. DsRed-positive profiles that overlapped in the 2D projections of the paired image stacks were identified, and their pixel areas were measured and converted to square micrometers with Fiji (18). Finally, sizes of stationary sites per unit axonal lengths were calculated and compared with compensate for the different sampling lengths of each axon. Some slice cultures were fixed, immunostained with proteolipid protein (Agmed) and/or APP antibodies, and examined by confocal microscopy as described previously (18). For each imaging experiment, slice culture data were collected from randomly selected axons in at least five slices obtained from three different animals.

Statistical Analyses. Statistical analyses including a normality test were performed by using SigmaStat (Aspire Software International). Data are presented as means with SEM for normally distributed data or medians with first-to-third quartile ranges. Comparisons were made by using the two-tailed Student *t* test for normally distributed data and the Mann–Whitney *U* test for nonparametric data. Multiple comparisons were performed with Bonferroni corrections.

NEUROSCIENCE

www.manaraa.com

1. Trapp BD, Nave KA (2008) Multiple sclerosis: An immune or neurodegenerative disorder? *Annu Rev Neurosci* 31:247–269.
2. Trapp BD, et al. (1998) Axonal transection in the lesions of multiple sclerosis. *N Engl J Med* 338(5):278–285.
3. Ferguson B, Matyszak MK, Esiri MM, Perry VH (1997) Axonal damage in acute multiple sclerosis lesions. *Brain* 120(Pt 3):393–399.
4. Bitsch A, Schuchardt J, Bunkowski S, Kuhlmann T, Brück W (2000) Acute axonal injury in multiple sclerosis. Correlation with demyelination and inflammation. *Brain* 123(pt 6):1174–1183.
5. Lassmann H, Brück W, Lucchinetti CF (2007) The immunopathology of multiple sclerosis: An overview. *Brain Pathol* 17(2):210–218.
6. Nave KA, Trapp BD (2008) Axon-glial signaling and the glial support of axon function. *Annu Rev Neurosci* 31:535–561.
7. Nave KA (2010) Myelination and support of axonal integrity by glia. *Nature* 468(7321):244–252.
8. Griffiths I, et al. (1998) Current concepts of PLP and its role in the nervous system. *Microsc Res Tech* 41(5):344–358.
9. Lappe-Siefke C, et al. (2003) Disruption of Cnp1 uncouples oligodendroglial functions in axonal support and myelination. *Nat Genet* 33(3):366–374.
10. Yin X, et al. (2006) Evolution of a neuroprotective function of central nervous system myelin. *J Cell Biol* 172(3):469–478.
11. Coleman M (2005) Axon degeneration mechanisms: Commonality amid diversity. *Nat Rev Neurosci* 6(11):889–898.
12. Trapp BD, Stys PK (2009) Virtual hypoxia and chronic necrosis of demyelinated axons in multiple sclerosis. *Lancet Neurol* 8(3):280–291.
13. Dutta R, et al. (2006) Mitochondrial dysfunction as a cause of axonal degeneration in multiple sclerosis patients. *Ann Neurol* 59(3):478–489.
14. Mahad DJ, et al. (2009) Mitochondrial changes within axons in multiple sclerosis. *Brain* 132(Pt 5):1161–1174.
15. Campbell GR, et al. (2011) Mitochondrial DNA deletions and neurodegeneration in multiple sclerosis. *Ann Neurol* 69(3):481–492.
16. Misgeld T, Kerschensteiner M, Bareyre FM, Burgess RW, Lichtman JW (2007) Imaging axonal transport of mitochondria in vivo. *Nat Methods* 4(7):559–561.
17. Kiryu-Seo S, Ohno N, Kidd GJ, Komuro H, Trapp BD (2010) Demyelination increases axonal stationary mitochondrial size and the speed of axonal mitochondrial transport. *J Neurosci* 30(19):6658–6666.
18. Ohno N, et al. (2011) Myelination and axonal electrical activity modulate the distribution and motility of mitochondria at CNS nodes of Ranvier. *J Neurosci* 31(20):7249–7258.
19. Saxton WM, Hollenbeck PJ (2012) The axonal transport of mitochondria. *J Cell Sci* 125(Pt 9):2095–2104.
20. Schwarz TL (2013) Mitochondrial trafficking in neurons. *Cold Spring Harb Perspect Biol* 5(6).
21. Chang DT, Reynolds IJ (2006) Mitochondrial trafficking and morphology in healthy and injured neurons. *Prog Neurobiol* 80(5):241–268.
22. Berman SB, et al. (2009) Bcl-x L increases mitochondrial fission, fusion, and biomass in neurons. *J Cell Biol* 184(5):707–719.
23. Sheng ZH, Cai Q (2012) Mitochondrial transport in neurons: Impact on synaptic homeostasis and neurodegeneration. *Nat Rev Neurosci* 13(2):77–93.
24. Kang JS, et al. (2008) Docking of axonal mitochondria by syntaphilin controls their mobility and affects short-term facilitation. *Cell* 132(1):137–148.
25. Misko AL, Sasaki Y, Tuck E, Milbrandt J, Baloh RH (2012) Mitofusin2 mutations disrupt axonal mitochondrial positioning and promote axon degeneration. *J Neurosci* 32(12):4145–4155.
26. Evangelou N, et al. (2000) Regional axonal loss in the corpus callosum correlates with cerebral white matter lesion volume and distribution in multiple sclerosis. *Brain* 123(pt 9):1845–1849.
27. Matsushima GK, Morell P (2001) The neurotoxicant, cuprizone, as a model to study demyelination and remyelination in the central nervous system. *Brain Pathol* 11(1):107–116.
28. Narayanan SP, Flores AI, Wang F, Macklin WB (2009) Akt signals through the mammalian target of rapamycin pathway to regulate CNS myelination. *J Neurosci* 29(21):6860–6870.
29. Suzuki K (1969) Giant hepatic mitochondria: Production in mice fed with cuprizone. *Science* 163(3862):81–82.
30. Flatmark T, Kryvi H, Tangerås A (1980) Induction of megamitochondria by cuprizone (biscyclohexanone oxaldihydrazone). Evidence for an inhibition of the mitochondrial division process. *Eur J Cell Biol* 23(1):141–148.
31. Blakemore WF (1973) Demyelination of the superior cerebellar peduncle in the mouse induced by cuprizone. *J Neurol Sci* 20(1):63–72.
32. Ludwin SK (1978) Central nervous system demyelination and remyelination in the mouse: An ultrastructural study of cuprizone toxicity. *Lab Invest* 39(6):597–612.
33. Tsai J, Grutzendler J, Duff K, Gan WB (2004) Fibrillar amyloid deposition leads to local synaptic abnormalities and breakage of neuronal branches. *Nat Neurosci* 7(11):1181–1183.
34. Nikić I, et al. (2011) A reversible form of axon damage in experimental autoimmune encephalomyelitis and multiple sclerosis. *Nat Med* 17(4):495–499.
35. Bjartmar C, Trapp BD (2001) Axonal and neuronal degeneration in multiple sclerosis: Mechanisms and functional consequences. *Curr Opin Neurol* 14(3):271–278.
36. Stys PK, Waxman SG, Ransom BR (1992) Ionic mechanisms of anoxic injury in mammalian CNS white matter: Role of Na+ channels and Na(+)-Ca2+ exchanger. *J Neurosci* 12(2):430–439.
37. Kapoor R, Davies M, Blaker PA, Hall SM, Smith KJ (2003) Blockers of sodium and calcium entry protect axons from nitric oxide-mediated degeneration. *Ann Neurol* 53(2):174–180.
38. Bechtold DA, et al. (2005) Axonal protection in experimental autoimmune neuritis by the sodium channel blocking agent flecainide. *Brain* 128(pt 1):18–28.
39. Skripuletz T, Gudi V, Hackstette D, Stangel M (2011) De- and remyelination in the CNS white and grey matter induced by cuprizone: The old, the new, and the unexpected. *Histol Histopathol* 26(12):1585–1597.
40. Mutsaers SE, Carroll WM (1998) Focal accumulation of intra-axonal mitochondria in demyelination of the cat optic nerve. *Acta Neuropathol* 96(2):139–143.
41. Sathornsumetee S, McGavern DB, Ure DR, Rodriguez M (2000) Quantitative ultrastructural analysis of a single spinal cord demyelinated lesion predicts total lesion load, axonal loss, and neurological dysfunction in a murine model of multiple sclerosis. *Am J Pathol* 157(4):1365–1376.
42. Witte ME, et al. (2009) Enhanced number and activity of mitochondria in multiple sclerosis lesions. *J Pathol* 219(2):193–204.
43. Waxman SG (2006) Axonal conduction and injury in multiple sclerosis: The role of sodium channels. *Nat Rev Neurosci* 7(12):932–941.
44. Fünfschilling U, et al. (2012) Glycolytic oligodendrocytes maintain myelin and long-term axonal integrity. *Nature* 485(7399):517–521.
45. Lee Y, et al. (2012) Oligodendroglia metabolically support axons and contribute to neurodegeneration. *Nature* 487(7408):443–448.
46. Persson AK, et al. (2013) Sodium channels contribute to degeneration of dorsal root ganglion neurites induced by mitochondrial dysfunction in an in vitro model of axonal injury. *J Neurosci* 33(49):19250–19261.
47. Lo AC, Saab CY, Black JA, Waxman SG (2003) Phenytoin protects spinal cord axons and preserves axonal conduction and neurological function in a model of neuroinflammation in vivo. *J Neurophysiol* 90(5):3566–3571.
48. Bechtold DA, Kapoor R, Smith KJ (2004) Axonal protection using flecainide in experimental autoimmune encephalomyelitis. *Ann Neurol* 55(5):607–616.
49. Stys PK (2005) General mechanisms of axonal damage and its prevention. *J Neurol Sci* 233(1-2):3–13.
50. Cardona A, et al. (2012) TrakEM2 software for neural circuit reconstruction. *PLoS ONE* 7(6):e38011.
51. Birgbauer E, Rao TS, Webb M (2004) Lysolecithin induces demyelination in vitro in a cerebellar slice culture system. *J Neurosci Res* 78(2):157–166.